Structure of B_2O_3 Glass at High Pressure: A ^{11}B Solid-State NMR Study

Sung Keun Lee,[1,*] Kenji Mibe,[2] Yingwei Fei,[2] George D. Cody,[2] and Bjorn O. Mysen[2]

[1]*School of Earth and Environmental Sciences, Seoul National University, Seoul, 151-742 Korea*
[2]*Geophysical Laboratory, Carnegie Institution of Washington, 5251 Broad Branch Road, NW, Washington, D.C., 20015, USA*
(Received 11 January 2005; published 29 April 2005)

We report spectroscopic evidence for the pressure-induced structural changes in B_2O_3 glass quenched from melts at pressures up to 6 GPa using solid-state NMR. While all borons are tri-coordinated at 1 atm, the fraction of tetra-coordinated boron increases with pressure, being about 5% and 27% in the B_2O_3 glass quenched from melts at 2 and 6 GPa, respectively. The fraction of boroxol ring species increases with pressure up to 2 GPa and apparently decreases with further compression up to 6 GPa. Two densification mechanisms are proposed to explain the variation of boron species with pressure.

PACS numbers: 62.50.+p, 61.43.Fs

B_2O_3 glass is one of the simplest glasses and has been extensively studied using various experimental and theoretical tools. It has also been explored in the context of the diverse range of boron containing optical materials and glass ceramics. Understanding boron structures in glasses is also of fundamental importance in the modification of the structure of other covalent oxide glasses. Minor fractions of B_2O_3 in magmatic melts could also play an important role in controlling transport properties and, thus, the dynamics of magmas. Whereas the state of intermediate-range order in B_2O_3 glass has historically been controversial, recent spectroscopic and scattering studies have confirmed that B_2O_3 glass consists of about 70% boroxol ring (3 membered planar ring $B_3O_6{}^{3-}$) and about 30% of nonring borons (e.g., [1–6]). The role of pressure on the structure and disorder in the archetypal B_2O_3 glass remains an unsolved question in condensed matter physics in spite of its fundamental importance to the dynamics of magmatic melts in the Earth's interior and for a broader understanding of pressure-induced structural changes in this archetypal glass as well as more complex covalent oxide glasses. Early Raman studies reported that the fraction of boroxol ring decreases with pressure above 6 GPa and suggested evidence for the permanent densification wherein the fraction of boroxol ring remains low upon decompression [7]. Earlier *in situ* Brillouin scattering studies reported changes in the wave velocity upon decompression of B_2O_3 glass initially compressed in the diamond anvil cell, which was recently confirmed by more detailed studies using Raman and Brillouin scattering [8,9]. These results imply some structural rearrangements at around 3 GPa, presumably from a transition from low- to high-density amorphous phases (e.g., polyamorphism) [9].

Recent solid-state NMR experiments, in particular, the triple quantum magic angle spinning (3QMAS) NMR, have been effective in resolving the atomic configurations surrounding quadrupolar nuclides (e.g., [11]B, [17]O, and [27]Al) in the crystalline and noncrystalline solids (e.g., [10–12]). Pressure-induced changes in coordination around framework cations such as Al and Si in silicate and aluminosilicate glasses have been recently investigated using [17]O and

^{27}Al 3QMAS NMR, unveiling details of aluminosilicate glass structure at high pressure [13–16]. In general, the primary densification mechanisms in these glasses involve changes in the fraction of nonbridging oxygens (NBO's). ^{11}B MAS NMR were recently applied to sodium borosilicate glasses revealing that the fraction of [4]B increases with pressure at the expense of NBO [17]. This trend is consistent with the results from ^{17}O 3QMAS NMR studies for aluminosilicate glasses and suggestions from pioneering ^{29}Si MAS NMR for silicate glasses at high pressure [16,18–21]. In the case of the pure B_2O_3 glasses, all the oxygen is bridging oxygen (BO); thus, different densification mechanisms would be necessary to impart structural changes to this glass at high pressures. Both ^{11}B MAS and 3QMAS NMR experiments are ideal to explore the pressure-induced changes in coordination and the topology of boron cluster. Here, we explore the structure of B_2O_3 glass quenched from melts compressed to pressures of up to 6 GPa in piston and a multianvil apparati using these solid-state NMR techniques.

B_2O_3 glass was synthesized from boric acid powder by heating (above 773 K) and quenching several times at 1 atm ($B_2O_3$1 atm glass) and was loaded in a piston cylinder for synthesis at 2 GPa ($B_2O_3$2 GPa glass) and in a multianvil apparatus with a 18/11 (octahedron edge length or truncated edge length of the anvils) assembly for the synthesis at 6 GPa ($B_2O_3$6 GPa glass). The samples were fused at 1273 (2 GPa) and 1773 K (6 GPa) for about 5 min and then quenched at those pressures. The structures of glasses represent those of supercooled melts at their glass transition temperature (T_g) and high pressure. It should be noted that the structure of cold-pressed glasses in diamond anvil cell (without heating) is not identical to that obtained by quenching of the liquids at high pressure [22,23]. The former does not undergo glass transition at high pressure and represent the densified glasses, and the latter represents the structure of supercooled liquids at high pressure at T_g. It also has been reported in the study of cold-pressed borate glass that pressure response of cold-pressed glass appeared to be slow, necessitating the equilibration time of about several hours [9,24]. On the other

hand, the equilibration of borate melts at high pressure should be much faster because the viscosity of melts (above melting temperature) is several orders of magnitude lower than that of glass.

^{11}B MAS and 3QMAS NMR spectra were collected on a Varian 600 spectrometer (14.1 T) at a Larmor frequency of 192.49 MHz. A 2.5 mm ZrO_2 rotor in Varian probe was used. The recycle delay for the MAS NMR experiments is 1 s, with radio frequency pulse lengths of 0.3 μs (about a 15° tip angle for the central transition in solids). ^{11}B 3QMAS NMR spectrum for B_2O_3 6 GPa glass was collected using a shifted-echo pulse sequence [two hard pulses with durations of 3.3 and 1.3 μs, and with a soft pulse (22 μs)] with a recycle delay of 2 s. ^{11}B 3QMAS NMR spectrum for B_2O_3 1 atm glass was reported previously [25] and shown here for comparison with a B_2O_3 6 GPa. The sample spinning speed was 19 kHz. The spectra were referenced to $BF_3(CH_3CH_2)_2O$.

Figure 1 shows ^{11}B MAS NMR spectra for B_2O_3 glasses quenched from melts at varying pressure. B_2O_3 glasses at 1 atm have been previously studied using NMR, which revealed that all the borons are tri-coordinated. The [3]B peak can be decomposed into a boroxol ring and a nonring component (see Fig. 3 for more details). There is no detectable [4]B, whose peak maximum is expected to be at $-0 \sim -3$ ppm at 14.1 T [1]. With increasing pressure to 2 GPa, the shape of [3]B cluster of quadrupolar line differs significantly from that at 1 atm, implying changes in fractions of boroxol ring and nonring [3]B. A peak at ~ -0 ppm corresponds to [4]B in the B_2O_3 glass ([3]B $\Leftrightarrow$ [4]B), revealing a pressure-induced change in coordination number of boron. The fraction of [4]B is about 5% at 2 GPa and increases with further increase in pressure to about 27% at 6 GPa. The chemical shift of [4]B peak at 6 GPa is smaller than [3]B. [4]B peak has shoulder at the higher frequency side (arrow in Fig. 1), suggesting several distinct
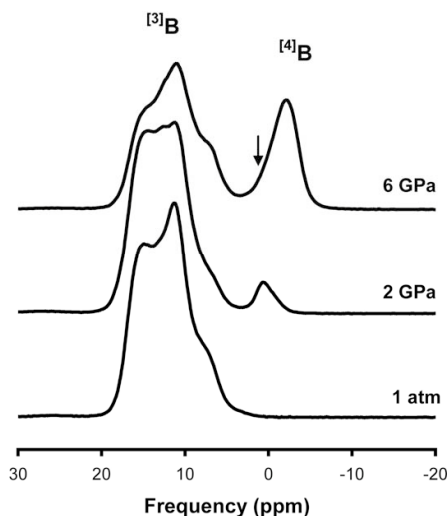
[4]B environments have formed with pressure. Note that the peak position highlighted with the arrow is consistent with the [4]B peak position for B_2O_3 2 GPa. The peak shape of [3]B spectral region is also apparently different from those at lower pressure. While it is evident in Fig. 1 that the there are substantial changes in atomic environments of [3]B, it is not yet clear whether this is due to the changes in the fractions of boroxol ring or variation of NMR parameters [e.g., isotropic chemical shift (δ_{iso}), quadrupolar coupling constant (C_q), and quadrupolar asymmetry parameter (η)] that could change peak shape with pressure.

Figure 2 presents the ^{11}B 3QMAS NMR spectra for B_2O_3 glasses quenched from melts at 1 atm and 6 GPa where the spectra for the 1 atm glasses showed partially resolved nonring and boroxol ring components as has been previously reported [25]. The B_2O_3 6 GPa glass reveals that the fraction of boroxol ring appears to decrease and η apparently increases with pressure: the projection to the MAS dimension is almost identical to the 1D ^{11}B MAS NMR. Therefore, the shape of the 2D NMR peak allows direct (albeit) qualitative comparison of the quadrupolar asymmetry parameter (η). The spectrum of the 1 atm glass in Fig. 2 reveals the well-developed quadrupolar pattern of both ring and nonring boron in the MAS dimension whereas the shape of [3]B peak of spectrum of the 6 GPa glass suggests a larger η. This is confirmed by the direct simulation of 1D MAS NMR spectrum (Fig. 3). These
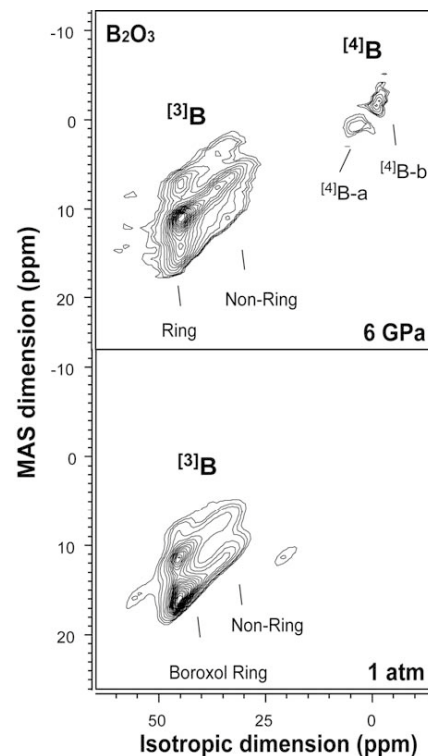

FIG. 2. ^{11}B 3QMAS NMR spectra for B_2O_3 glasses quenched from melts at 1 atm 25 and 6 GPa. Contour lines are drawn from 8% to 93% of relative intensity with a 5% increment and added lines at 4 and 6%.

FIG. 1. ^{11}B MAS NMR spectra for B_2O_3 glasses quenched from melts at varying pressures as labeled.

results demonstrate that the changes in line shape of the ^{11}B MAS NMR spectra for B_2O_3 glasses at 6 GPa stems from both a variation in ring/nonring ratio as well as the changes in structurally relevant NMR parameters, particularly η with pressure. There are also two resolved [4]B sites in B_2O_3 6 GPa, which is consistent with the prediction from peak shape of [4]B peak for ^{11}B MAS NMR spectrum at 6 GPa. The site [4]B-*a* may be due to [4]B primarily coordinated by [3]B in the boroxol ring or nonring as next nearest neighbors. The site labeled [4]B-*b* is likely to correspond to [4]B sites whose next nearest neighbors have more fractions of nonring or [4]B. Note that the fractions of [4]B sites in the 3QMAS NMR spectrum are smaller than the populations obtained from MAS NMR due to the smaller C_q for these sites compared with [3]B: the 3QMAS efficiency drops significantly for the sites with small C_q (e.g., <1 MHz) (e.g., [12]).

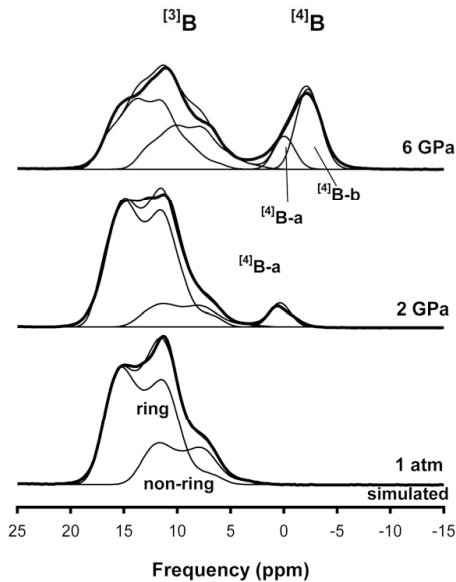Using the NMR parameters obtained from the peak positions and centers of gravity of the peaks from [11]B

FIG. 3. Simulation of ^{11}B MAS NMR spectra for B_2O_3 glasses using the following NMR parameters (thin lines). Thick lines refer to the experimental ^{11}B MAS NMR spectra. Final NMR parameters δ_{iso}(ppm):C_q(MHz):η for the simulations are 18.2 ± 0.3, 2.7 ± 0.1, 0.25 ± 0.05 for [3]B ring_1 atm; 14.6 ± 0.3, 2.7 ± 0.1, 0.25 ± 0.05 for [3]B nonring_1 atm; 18.2 ± 0.3, 2.7 ± 0.2, 0.35 ± 0.1 for [3]B ring_2 GPa; 14.6 ± 0.3, 2.7 ± 0.2, 0.25 ± 0.1 for [3]B nonring_2 GPa; 1 ± 0.3, <1 MHz, η cannot be uniquely defined for [4]B-*a*2 GPa; 17.8 ± 0.4, 2.65 ± 0.2, 0.52 ± 0.05 for [3]B ring_6 GPa; 14.1 ± 0.4, 2.65 ± 0.2, 0.52 ± 0.05 for [3]B nonring_6 GPa; 1 ± 0.3, <1 MHz for [4]B-*a*6 GPa; −0.8 ± 0.3, <1 MHz for [4]B-*b*6 GPa. Here, the uncertainty in η was determined from the simulation of [3]B peak shape with 6 NMR parameters (δ_{iso}, C_q, η) for both ring and nonring boron sites. The uncertainty of η can be larger (e.g., 0.1) if we consider the possible variation of η value for a boron site without constraining both boron sites simultaneously.

3QMAS NMR as input parameters, we simulated ^{11}B MAS NMR spectra for v-B_2O_3. Figure 3 shows simulation results of the MAS spectra (the caption to Fig. 3 shows the NMR parameters obtained from the simulation of ^{11}B MAS NMR spectra). As mentioned above, ^{11}B MAS NMR spectra for v-B_2O_3 1 atm are decomposed into boroxol ring and nonring component. At 2 GPa, [3]B can be decomposed into two components and the fraction of boroxol ring apparently increases. Whereas C_q and δ_{iso} of each component do not change much with pressure, η increases significantly with pressure. At 6 GPa, the η of both ring and nonring appears to be more than 0.5 compared with 0.25 for the both species at 1 atm. This suggests changes in both the ring and nonring topology, most likely distortion of the boron oxide triangle stemming from the increases in bond angle (O-B-O) and length (B-O), which leads to the increase in topological disorder [16]. These results provide experimental evidence for the pressure-induced changes in the coordination and topology in the B_2O_3 glasses. While the higher η boron site at high pressure partly stems from the larger distortion in boron sites associated with topological increased disorder, detailed correlation between topology and η remains to be explored, particularly using systematic quantum chemical calculations. Higher η sites were reported from crystalline calcium metaborates where NBO is present in the boron coordination shell [26]. While no NBO is likely to be present at the B_2O_3 glasses at high pressure, it seems that [3]B sites in these glasses tend to have tricluter oxygen (triply bonded oxygen, [tr]O) in their coordination shell as suggested from a recent synchrotron inelastic x-ray scattering study [27], and thus the B-O bond length of [3]B-[tr]O could be longer than [3]B-O, leading to an increase in the asymmetry of the boron sites and thus the η at high pressure.

Figure 4 presents the fraction of boron species with pressure obtained from the simulation of spectra as shown in Fig. 3 where [4]B clearly increases with pressure. Whereas the [3]B fraction decreases with pressure, the fraction of the boroxol ring apparently increases with pressure up to 2 GPa and then decreases with further increases in pressure. It is likely that the fraction of boroxol rings will decrease with further increases in pressure as has been reported from the earlier Raman studies [8,9].

Considering the above results, the densification mechanism related to boroxol ring formation may be described by the following two different schemes. In the lower pressure regime (below 2 GPa),

$$\text{Nonring } ([3]B) \Rightarrow \text{ Ring } ([3]B) + [4]B. \qquad (1)$$
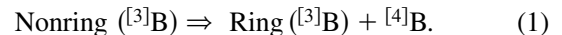
This scheme could be related to the reduction of bond angle with pressure and thus the subsequent formation of ring component (smaller B-O-B angle) from the nonring component (larger bond angle) [25], which decreases free volume and leads to an increase in the coordination number of borons with pressure. Also note that [4]B, at the lower pressure, mainly associates with [3]B as next nearest neigh-
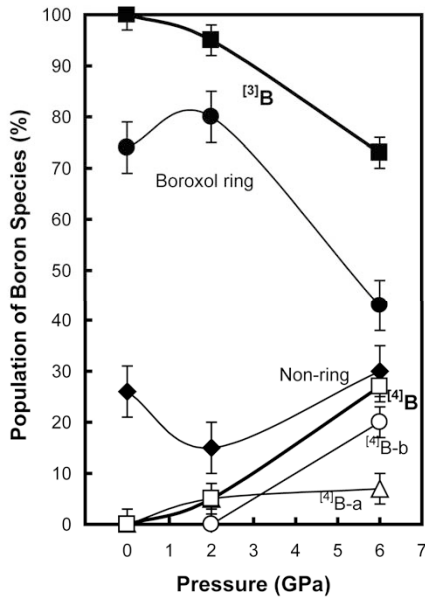
FIG. 4. Population of boron species for B_2O_3 glasses with pressure. Closed square, circle, and diamond refer to total [3]B population, [3]B ring, and [3]B nonring, respectively. Open squares, triangles, and circles denote total [4]B, [4]B-*a*, and [4]B-*b*, respectively.

bors ([4]B-*a*). At the higher pressures as shown in Fig. 4, the following scheme serves to describe the changes in the boron species:

$$\text{Ring } (^{[3]}\text{B}) \Rightarrow \text{ Nonring } (^{[3]}\text{B}) + {}^{[4]}\text{B}. \qquad (2)$$
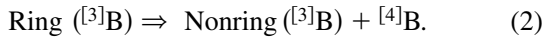
These schemes are consistent with previous observations of a decrease in boroxol ring concentration with pressure above 6 GPa and with our previous investigation using inelastic x-ray scattering studies at high pressure: an unpaired *p* orbital in oxygen could contribute to form [4]B due to a σ bond with a p_z orbital in the [3]B in the boroxol ring, as evidenced by the recent *in situ* synchrotron inelastic x-ray scattering of v-B_2O_3 with pressure [27] where [4]B fraction increases with pressure.

In summary, we report the first direct NMR evidence of the formation of [4]B with pressure in B_2O_3 glasses at high pressure and show pressure-induced changes in topology, particularly, in the ring/nonring fraction. The densification mechanism may be described by the topological variation at lower pressure (e.g., below 2 GPa) and then in changes in coordination above 2 GPa. Both mechanisms involve the interconversion between ring and nonring. Together with our recent results from synchrotron inelastic scattering, the results and methodology given here provide enhanced understanding of the pressure-induced structural changes in the archetypal glass forming liquids and may provide a microscopic explanation for the densification in the covalent oxide melts [20].

NMR spectra were collected at 600 MHz NMR facility at Korean Basic Science Institute (Tae-Gu center).

*Corresponding author. Email: sungklee@snu.ac.kr
[1] P. J. Bray, J. Non-Cryst. Solids **73**, 19 (1985).
[2] C. Joo, U. Werner-Zwanziger, and J. W. Zwanziger, J. Non-Cryst. Solids **261**, 282 (2000).
[3] A. C. Hannon, D. I. Grimley, R. A. Hulme *et al.*, J. Non-Cryst. Solids **177**, 299 (1994).
[4] A. C. Wright, S. A. Feller, and A. C. Hannon, *Borate Glasses, Crystals, and Melts* (Society of Glass Technology, Sheffield UK, 1996).
[5] R. E. Youngman, S. T. Haubrich, J. W. Zwanziger *et al.*, Science **269**, 1416 (1995).
[6] J. Swenson and L. Borjesson, Phys. Rev. B **55**, 11138 (1997).
[7] M. Grimsditch, A. Polian, and A. C. Wright, Phys. Rev. B **54**, 152 (1996).
[8] M. Grimsditch, R. Bhadra, and Y. Meng, Phys. Rev. B **38**, 7836 (1988).
[9] J. Nicholas, S. Sinogeikin, J. Kieffer *et al.*, Phys. Rev. Lett. **92**, 215701 (2004).
[10] J.-P. Amoureux, F. Bauer, H. Ernst *et al.*, Chem. Phys. Lett. **285**, 10 (1998).
[11] P. J. Dirken, S. C. Kohn, M. E. Smith *et al.*, Chem. Phys. Lett. **266**, 568 (1997).
[12] I. Frydman and J. S. Harwood, J. Am. Chem. Soc. **117**, 5367 (1995).
[13] J. R. Allwardt, B. C. Schmidt, and J. F. Stebbins, Chemical Geology **213**, 137 (2004).
[14] S. K. Lee, Y. Fei, G. D. Cody *et al.*, Geophys. Res. Lett. **30**, 1845 (2003).
[15] S. K. Lee, G. D. Cody, Y. Fei *et al.*, Geochim. Cosmochim. Acta **68**, 4203 (2004).
[16] S. K. Lee, J. Phys. Chem. B **108**, 5889 (2004).
[17] L. S. Du, J. R. Allwardt, B. C. Schmidt *et al.*, J. Non-Cryst. Solids **337**, 196 (2004).
[18] X. Xue, J. F. Stebbins, M. Kanzaki *et al.*, Am. Mineral. **76**, 8 (1991).
[19] X. Xue, J. F. Stebbins, and M. Kanzaki, Am. Mineral. **79**, 31 (1994).
[20] B. T. Poe, P. F. McMillan, D. C. Rubie *et al.*, Science **276**, 1245 (1997).
[21] J. L. Yarger, K. H. Smith, R. A. Nieman *et al.*, Science **270**, 1964 (1995).
[22] R. J. Hemley, C. Meade, and H. K. Mao, Phys. Rev. Lett. **79**, 1420 (1997).
[23] G. H. Wolf and P. F. McMillan, in *Structure, Dynamics, and Properties of Silicate Melts*, edited by J. F. Stebbins, P. F. McMillan, and D. B. Dingwell (Mineralogical Society of America, Washington, DC, 1995), Vol. 32, p. 505.
[24] A. C. Wright, C. E. Stone, R. N. Sinclair *et al.*, Phys. Chem. Glasses **41**, 296 (2000).
[25] S. K. Lee, C. B. Musgrave, P. Zhao *et al.*, J. Phys. Chem. B **105**, 12583 (2001).
[26] H. M. Kritz, S. G. Bishop, and P. J. Bray, J. Chem. Phys. **49**, 557 (1968).
[27] S. K. Lee, P. J. Eng, H. K. Mao *et al.* (to be published).